ATMOSPHERIC SCIENCE LETTERS
Atmos. Sci. Let. **18**: 475–483 (2017)
Published online in Wiley Online Library
(wileyonlinelibrary.com) **DOI:** 10.1002/asl.791

RMetS
Royal Meteorological Society

The underestimated magnitude and decline trend in near-surface wind over China

Ying Jiang,[1] Xiyan Xu,[2,3]* Hanwu Liu,[4] Xuguang Dong,[5] Wenben Wang[4] and Gensuo Jia[2]

[1]*Specialized Meteorological Office, Public Weather Service Center, China Meteorological Administration, Beijing, China*
[2]*CAS Key Laboratory of Regional Climate-Environment for Temperate East Asia, Institute of Atmospheric Physics, Chinese Academy of Sciences, Beijing, China*
[3]*Climate and Ecosystem Sciences Division, Lawrence Berkeley National Laboratory, Berkeley, CA, USA*
[4]*Meteorological Bureau of Chaohu Lake Basin, Chaohu, China*
[5]*Shandong Climate Center, Shandong Meteorological Bureau, Jinan, China*

*Correspondence to:
X. Xu, CAS Key Laboratory of Regional Climate-Environment for Temperate East Asia, Institute of Atmospheric Physics, Chinese Academy of Sciences, #40 Hua Yan Li, P. O. Box 9804, Chaoyang District, Beijing 100029, China.
E-mail: xiyan.xu@tea.ac.cn

Received: 28 April 2017
Revised: 26 July 2017
Accepted: 11 October 2017

Abstract

This study reports the magnitude, spatial pattern and temporal trend of near-surface wind speed (NWS) by comparing 20th century simulations in Coupled Model Intercomparison Project phase 5 (CMIP5) and 3 (CMIP3) and the climate reanalyses with measurements at 563 weather stations in China over 1961–2005. Both CMIP5 and CMIP3 agree quite well with observations in reproducing the spatial pattern of annual mean NWS. CMIP5 models are superior to CMIP3 models in hindcasting the magnitude and spatial pattern of seasonal mean NWS, the temporal trend in annual and seasonal mean NWS. Although both CMIP3 and CMIP5 reproduced the decline trend in the annual and seasonal mean NWS, the hindcasted decline rate is smaller than observed decline trend by the magnitude of one order. The ensemble of optimal models that are better correlated to observations in both NWS and temporal trend possesses advantages over individual model hindcast and reanalyses. The reanalyzed data are not able to represent the observed either the spatial pattern or the decline trend of NWS. The analyses presented here reveal the uncertainties in the current wind field products including reanalyses and model outputs and highlight the benefits of parameterization development and increased horizontal resolution in the new-generation CMIP models.

Keywords: **CMIP5; CMIP3; reanalysis; near-surface wind speed (NWS); model evaluation; China**

1. Introduction

The rise in economic activities increases the demand for energy. According to Wind Energy Foundation, wind energy is the fastest-growing energy source in the world for its clean, sustainable and affordable nature. In 2015, globally installed wind energy capacity is estimated as 60 GW, an increase of 16% from 2014 (Font, 2016). Early estimates indicate that China contributed about 42% of the 2015 globally installed capacity. The changes in wind exert direct impact on the wind energy density and thus wind power generation potential (Jiang *et al.,* 2010a).

Wind energy availability is susceptible to environmental change (Ren, 2010). In the past half-century, the global wind resources experienced significant change. In latitude >70°, near-surface wind speed (NWS) was enhanced over recent decades (Lynch *et al.,* 2004). In contrast, the observed NWS declined by 5–12% from 1979 to 2008 over northern mid-latitude continents (Vautard *et al.,* 2010). The decline trend has been observed in mid-latitude of Australia (McVicar *et al.,* 2008), Europe (Pryor *et al.,* 2012), North America (Pryor *et al.,* 2009) and China (Table S1, Supporting information). Both the annual and seasonal NWS has declined in China (Table S1). China Meteorological Administration (CMA) estimated the decline trend of 0.18 ms^{-1} per decade ($decade^{-1}$) from 1961 to 2014 in the country (CMA, 2015). In regions rich in wind resources, the winds slowed even stronger. On the Tibetan Plateau and northern China, the annual mean NWS declined at 0.24 ms^{-1} $decade^{-1}$ over 1980–2005 (You *et al.,* 2010) and 0.2 ms^{-1} $decade^{-1}$ over 1961–2014 (CMS, 2015), respectively. The decline trend in China is larger than that in Europe and North America (Vautard *et al.,* 2010).

The objective of CMIP is to better understand the past, present and future climate via model evaluation and improvement. CMIP5 ensemble mean captures the spatial variability of annual maximum NWS except in mountainous terrains while the historical trend of extreme wind is not well represented (Kumar *et al.,* 2015). While in China, all the CMIP5 models hindcasted lower interannual variability than reanalyses and observations (Chen *et al.,* 2012). Most CMIP3 models are able to simulate the distribution of wind resource in China but fail to simulate the NWS and the decline trend over the past 5 decades (Jiang *et al.,* 2010b). CMIP5

is superior to CMIP3 in simulating East Asian climate, such as Asian summer and winter Monsoons (Sperber *et al.,* 2013; Ogata *et al.,* 2014) and East Asian precipitation (Kusunoki and Arakawa, 2015).

In this study, we aim to evaluate how reliable the NWS products to represent the magnitude and trend of NWS and improvements of CMIP5 over CMIP3. We evaluate hindcasts of CMIP5 NWS in China against observation and reanalyses. We also perform an intercomparison of CMIP5 and CMIP3 simulations of spatial pattern of annual and seasonal NWS, and NWS trend over 1961–2005 in China. Section 2 outlines the observational, model and reanalyses data for intercomparison. Section 3 reports the simulated and observed NWS. Discussions and conclusions of those key findings are presented in Section 4.

2. Data and method

2.1. Data

We use NWS data measured at 10 m aboveground from January 1961 to December 2005 at 535 weather stations in China (Figure S1). In addition to the nationwide wind characteristics, we also evaluate the wind in five subregions (Figure S1). The quality control and subregions are given in Appendix S1.

We use three reanalysis datasets of monthly mean NWS at 10 m (Appendix S1): National Centers for Environmental Prediction/National Center for Atmospheric Research (NCEP/NCAR) reanalysis (Kalnay *et al.,* 1996), European Centre for Medium-Range Weather Forecasts (ECMWF) Reanalyses ERA-Interim (Berrisford *et al.,* 2009) and ERA-40 (Uppala *et al.,* 2005).

We analyze the 20th century simulations performed by models participating in CMIP3 (Meehl *et al.,* 2007) and CMIP5 (Taylor *et al.,* 2012) (Appendix S1). Twenty-three CMIP5 simulations over the period 1961–2005 and 19 CMIP3 simulations expanded from Jiang *et al.* (2010b) over the period 1956–1999 are used (Table S2).

2.2. Methods

The observations, reanalyses and CMIP simulations are regrided to $1^\circ \times 1^\circ$ spatial resolution by inverse distance weighting method (Isaaks and Srivastava, 1989) for intercomparison. Pearson correlation coefficient (PCC) between simulated and observed annual mean NWS distributed in the same $1^\circ \times 1^\circ$ grids is calculated to evaluate the models' hindcasts of NWS and spatial pattern. The trend of NWS is calculated by the linear regression of annual and seasonal mean NWS time series. We use PCC between time series of simulated and observed NWS at regional and nationwide scales to evaluate the models' hindcasts of interannual variability of seasonal and annual NWS. Furthermore, we evaluate the ensemble (multi-model mean) of all the models (All_M_Ens), the ensemble of the models in which the annual mean NWS is correlated to observations with confidence interval (CI) = 99.9% (Opt_S_Ens) and similar for the wind trend (Opt_T_Ens). The models participating in each ensemble analysis are listed in Table S3. The partition of the subregions for CMIP5 is the same as the region partition to observations. The partition of the subregions for CMIP3 remains the same as the partition in Jiang *et al.* (2010b).

3. Results

3.1. Spatial pattern of annual mean wind

In China, strong wind presents in northern and coastal regions in relative to weak wind in southern and inland regions of China. One weak wind zones is in Xinjiang and another one is across China starting from Hetao in Northwestern to Southern China via Sichuan basin. The strong wind zones are Tibetan plateau, the southern parts of northern and northeastern China and southeastern coastal areas. CMIP5 simulated spatial pattern of mean NWS agrees well with observations (Figure S2), which are successfully reproduced by most models. The correlation between the simulated and observed annual mean NWS in all grids is >0.25 (CI = 99%) in 19 of the 23 (83%) CMIP5 models, in which PCC is >0.32 (CI = 99.9%) in 6 models (Table 1). The ensemble of all the model hindcasts (All_M_Ens) and ensemble of the six optimal models (Opt_S_Ens) successfully represent the spatial pattern of NWS (Figure 1). PCC of Opt_S_Ens and All_M_Ens with observations are 0.47 (CI = 99.9%) and 0.36 (CI = 99.9%), respectively. ERA-interim is better correlated with observations (PCC = 0.45, CI = 99.9%), in comparison with ERA-40 (PCC = 0.26, CI = 99%) and NCEP/NCAR (PCC = 0.17).

Only 9 in 19 (47%) CMIP3 hindcasts are well correlated to observations (PCC > 0.25, CI = 99%) (Table 1). The models in CMIP5, in particular, HadGEM2-ES, MRI_CGCM3 and GISS-E2-R show significantly improved capture of the spatial pattern of mean NWS. Even so, All_M_Ens and Opt_S_Ens in CMIP5 show slight improvement compared to CMIP3 due to worse hindcasts in six CMIP5 models.

3.2. Magnitude of annual mean wind speed

The observed mean NWS over 1961–2005 is $2.41 \pm 0.2\,\mathrm{ms}^{-1}$. CMIP5 models tend to underestimate the annual mean NWS. Seventeen models have biases (simulations minus observations) within $\pm 1\,\mathrm{ms}^{-1}$, in which seven models have the biases within $\pm 0.5\,\mathrm{ms}^{-1}$ (Table 1). The hindcast by BNU-ESM is $2.45 \pm 0.07\,\mathrm{ms}^{-1}$, the closest to observations. Despite the relatively low bias in nationwide annual mean NWS, these models show a similar pattern of bias: overestimation in southwest and underestimation in other parts of China (Figure 2).

The observed annual mean NWS is the strongest in northeast ($2.97 \pm 0.25\,\mathrm{ms}^{-1}$), followed by northwest

Table 1. PCC between simulated and observed mean NWS in each grid cell, trend of annual mean NWS and mean NWS by individual model hincasts, ensemble model hindcasts and reanalyses.

No.		PCC		Trend of wind speed (ms^{-1} per decade)		Mean wind speed ± Standard deviation[a] (ms^{-1})	
Data		CMIP5	CMIP3	CMIP5	CMIP3	CMIP5	CMIP3
1	ACCESS1.3	0.38[b]	–	0.0[c]	–	2.01 ± 0.05	–
2	CSIRO-Mk3.6.0	0.30[d]	0.36[b]	−0.01[e]	0.00[e]	2.31 ± 0.06	2.45 ± 0.08
3	CanESM2	0.26[d]	0.17	0.02[f]	−0.01[c]	2.74 ± 0.08	2.72 ± 0.06
4	BCC-CSM1.1	0.29[d]	0.41[b]	0[c]	−0.05[e]	2.27 ± 0.06	3.55 ± 0.11
5	BNU-ESM	0.29[d]	–	−0.03[e]	–	2.45 ± 0.07	–
6	FGOALS-gl	0.05	0.32[b]	−0.01[c]	0.00	3.88 ± 0.12	3.67 ± 0.09
7	EC-EARTH	0.48[b]	–	0.00	–	1.76 ± 0.06	–
8	HadGEM2-ES	0.44[b]	0.17	0.00	−0.01[e]	1.21 ± 0.04	1.34 ± 0.04
9	CNRM-CM5	0.37[b]	0.30[d]	0.00[c]	0.00[c]	1.56 ± 0.05	0.92 ± 0.02
10	IPSL-CM5A-LR	0.25[d]	–	0.02[f]	–	1.85 ± 0.06	–
11	IPSL-CM5A-MR	0.27[d]	0.43[b]	0.02[f]	0.00	1.87 ± 0.06	0.82 ± 0.02
12	MPI-ESM-LR	0.31[d]	–	0.00[c]	–	1.40 ± 0.04	–
13	MPI-ESM-MR	0.28[d]	0.21	0.01	0.00	1.41 ± 0.05	1.33 ± 0.05
14	MIROC5	0.31[d]	0.30[d]	−0.01[c]	0.00	1.97 ± 0.07	2.19 ± 0.06
15	MIROC-ESM	0.26[d]	0.38[b]	0.03[f]	0.00[c,f]	2.20 ± 0.07	2.32 ± 0.05
16	MRI-CGCM3	0.37[b]	0.10	0.01[f]	0.00[e]	2.23 ± 0.06	1.74 ± 0.05
17	HadGEM2-AO	0.31[d]	–	−0.01[c]	–	1.27 ± 0.03	–
18	INM-CM4	0.23	0.23	0.00[c]	0.01	1.77 ± 0.05	1.93 ± 0.05
19	GFDL-ESM2M	0.26[d]	0.40[b]	−0.01[c]	0.01[c]	1.30 ± 0.05	1.34 ± 0.04
20	GFDL-CM3	0.19	0.27[d]	0.01	0.01	1.43 ± 0.05	1.42 ± 0.04
21	GISS-E2-H	0.24	0.17	0.01[f]	0.00[c]	1.57 ± 0.04	1.40 ± 0.03
22	GISS-E2-R	0.32[b]	0.17	0.00	0.00[c]	1.46 ± 0.03	1.45 ± 0.03
23	NorESM1-M	0.25[d]	0.17	−0.03[c]	0.01[f]	3.83 ± 0.09	0.89 ± 0.03
24	All_M_Ens	0.36[b]	0.34[b]	0.00	0.00	1.99 ± 0.72	1.85 ± 0.86
25	Opt_S_Ens	0.47[b]	0.43[b]	0.01[f]	0.00[e]	1.71 ± 0.37	2.36 ± 1.14
26	Opt_T_Ens	0.33[b]	–	−0.02[e]	0.00[e]	2.19 ± 0.94	–
27	ERA-40	0.26[d]	–	0.00	–	1.45 ± 0.04	–
28	ERA-interim	0.45[b]	–	−0.03		1.64 ± 0.06	–
29	NCEP/NCAR	0.17	–	−0.17	–	2.72 ± 0.28	–
30	Station	–	–	−0.13	−0.13	2.41 ± 0.20	2.47 ± 0.18

CMIP5 data is over 1961–2005 and CMIP3 data is over 1956–1999.

[a]For individual model, reanalyses and station measurements, the standard deviation is calculated from annual mean wind speed over 54 years; for ensembles, the standard deviation is calculated from the mean wind speed by individual model.

[b]PCC > 0.32 and CI of 99.9%.

[c]Trend with PCC > 0.

[d]PCC > 0.25 and CI of 99%.

[e]Trend with PCC > 0.29 and CI of 95%.

[f]Trend with CI of 90%.

($2.55 \pm 0.27\,ms^{-1}$), southwest ($2.3 \pm 0.26\,ms^{-1}$) and southeast ($2.27 \pm 0.18\,ms^{-1}$) of China. The weakest wind ($1.7 \pm 0.09\,ms^{-1}$) is observed in southern China. Given scarce observations and difficulties in simulating NWS on the Tibetan Plateau, we skip the southeastern region in CMIP5 NWS ranking. CMIP5 models of BCC-CSM1.1, BNU-ESM, CanESM2, GISS-E2-H, GISS-E2-R, HadGEM2-ES and NorESM1-M successfully reproduced the regional NWS from strongest to weakest in the order of northeast, northwest, southeast and south. ERA-interim is superior to ERA-40 and NCEP/NCAR in representing the spatial pattern (Table 1), but notably underestimates NWS (Figure 1(e)).

Similar to CMIP5, most CMIP3 models underestimate annual NWS. CMIP3 indicates that the underestimate is usually between 1 and $2\,ms^{-1}$. In some regions, the bias is up to $3\,ms^{-1}$. Only 36.8% of CMIP3 models hindcasted annual mean NWS biases within (−1 to 0) ms^{-1} compared to 60.9% of CMIP5 models and 5.3% of CMIP3 models hindcasted biases within (0–1) ms^{-1} compared to 8.7% of CMIP5 models (Figure S3). Bias of Opt_S_Ens for CMIP3 is smaller than CMIP5 (Figure S3(b)). However, this smaller bias is not contributed by better model skill but the spread hindcasts NWS among CMIP3 models (Table 1).

3.3. Seasonal mean wind speed

Seasonally, although most CMIP5 models can reproduce the nationwide spatial pattern of NWS, the magnitude is biased. Most models hindcasted NWS in spring, summer and fall approximate to or smaller than the observations, except FGOALS-gl, CanESM2 and NorEMS1-M (Figure 3(b)). The hindcasts of winter NWS are approximate to or larger than observations. The overestimate of nationwide winter mean NWS by CSIRO-Mk3.6.0, CanESM2, BNU-ESM, FGOALS-gl, MIROC-ESM and NorESM1-M is over $1\,ms^{-1}$. The

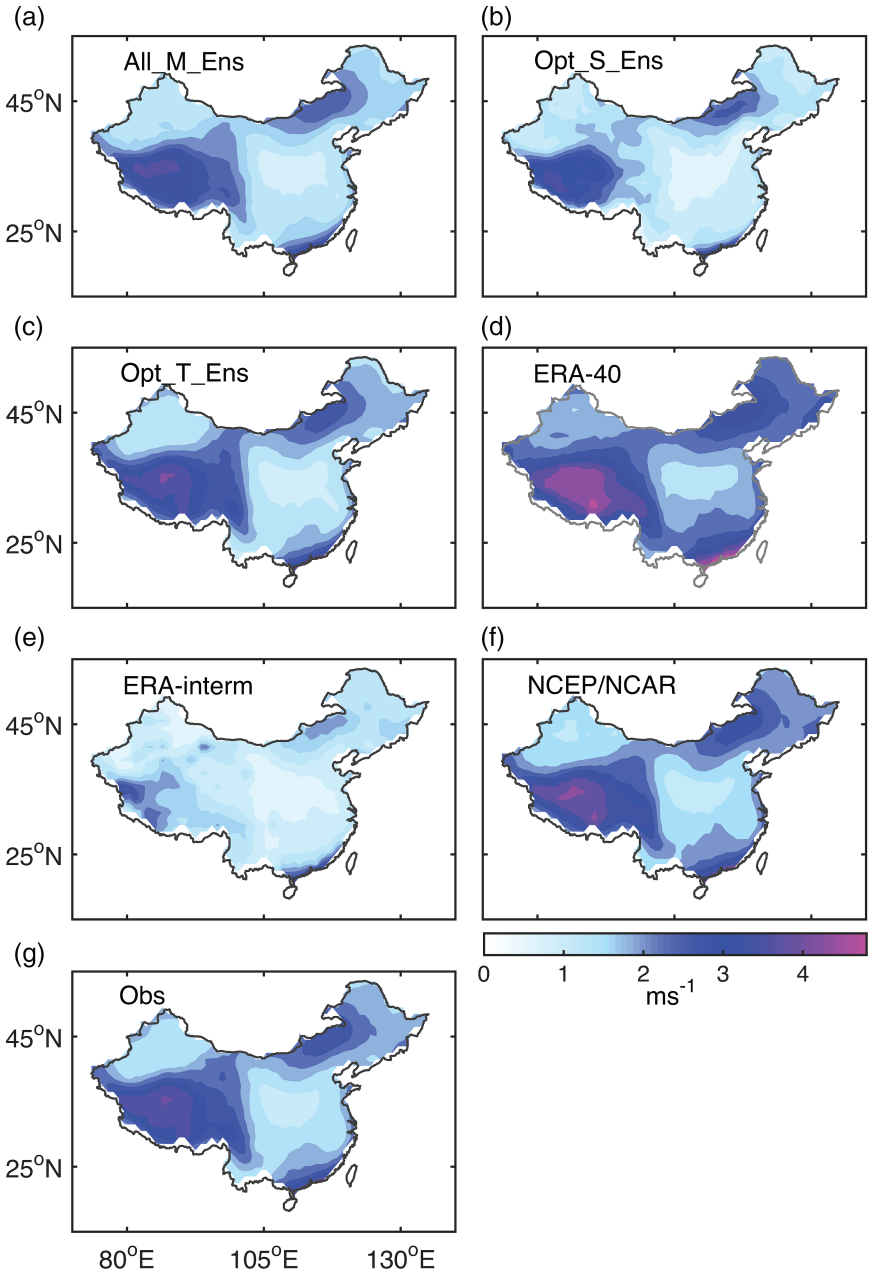

Figure 1. Distributions of mean wind speed (averaged over 1961–2005) for ensemble of all CMIP5 models (a), ensemble of optimal wind (b), ensemble of optimal trend (c), reanalyses (d–f) and observations (g) over mainland China.

correlations between simulated and observed seasonal pattern demonstrate that the spatial pattern in winter is best hindcasted, followed by fall, spring and summer. CMIP5 is superior to CMIP3 in not only the number of models that can hindcast the spatial pattern but also correlations between the model ensemble and observations in the seasonal scale (Table S4). Magnitude of NWS bias is reduced in CMIP5 for all the seasons (Figure S4).

3.4. Trend in annual and seasonal mean wind speed

The observed NWS over 1961–2005 is declined at $-0.13\,\mathrm{ms}^{-1}$ decade^{-1} (Table S5). The nationwide annual mean NWS is positively correlated to observations in 13 out of 23 CMIP5 models (Figure 3(a)), in which CSIRO-Mk3.6.0 and BNU-ESM have the correlations over 0.3 (CI = 95%). Most of CMIP5 and CMIP3 models hindcasted the decline trend, but smaller by one order of magnitude than observations (Table 1, Figure 4). NCEP/NCAR hindcasted the nationwide decline trend in the same order as the observations, however, it fails to represent the observed spatial pattern of NWS. All reanalyses presented low trend correlation with observations.

The observed decline trend is most significant in NNW ($-0.18\,\mathrm{ms}^{-1}$ decade^{-1}) and NE ($-0.17\,\mathrm{ms}^{-1}$ decade^{-1}), followed by SSE ($-0.13\,\mathrm{ms}^{-1}$ decade^{-1}), SW ($-0.07\,\mathrm{ms}^{-1}$ decade^{-1}) and CW ($-0.04\,\mathrm{ms}^{-1}$ decade^{-1}). Seven in 23 (30.4%) CMIP5 models hindcasted decline trend in mean NWS, in which

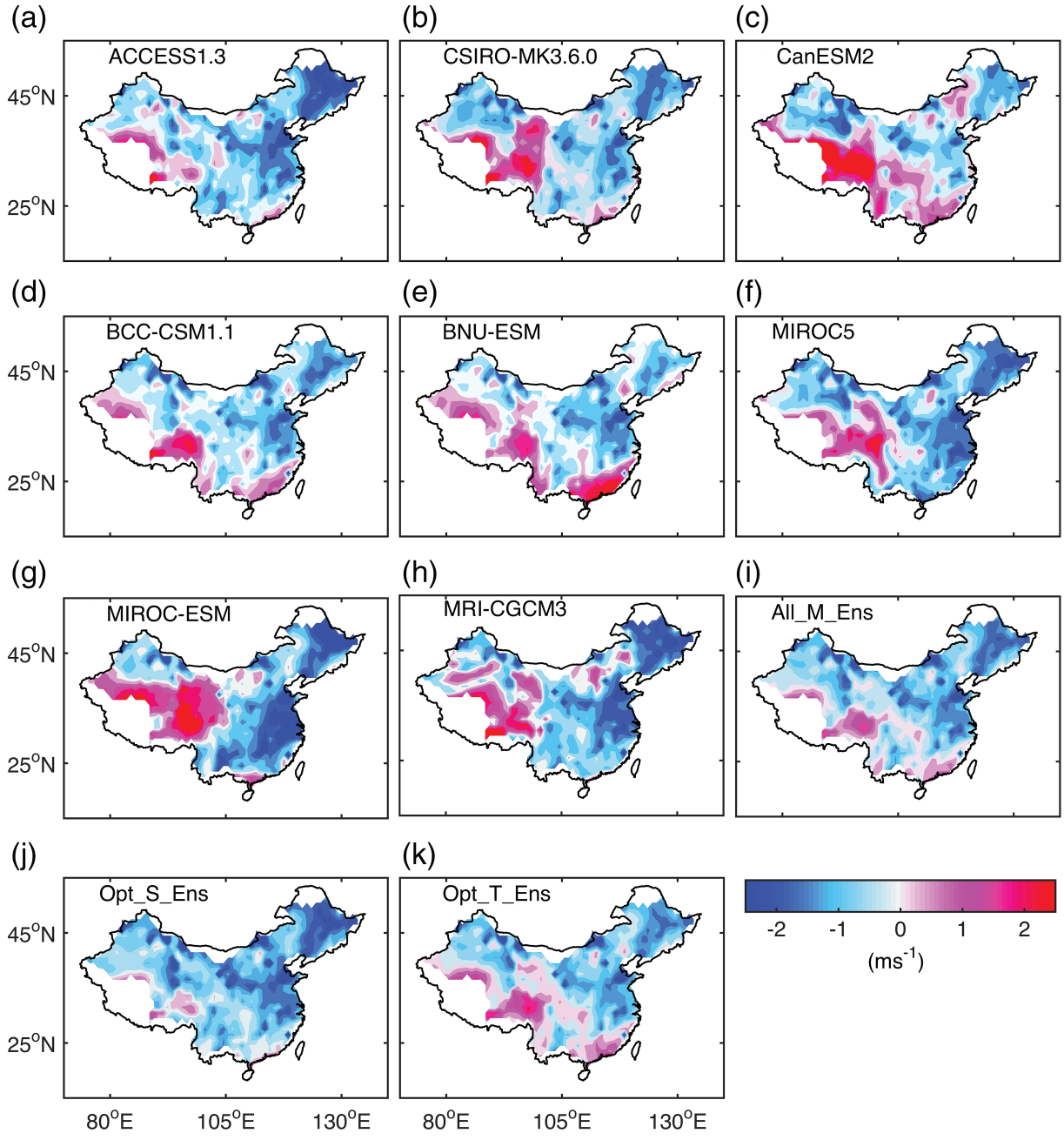

Figure 2. The predicted wind speed biases from observations in the individual model that have annual biases within ±0.5 ms^{-1} (a–h) and ensembles (i–k) over mainland China.

CSIRO-MK3.6.0 and BNU-ESM show CI = 95%, while 3 in 19 (17.6%) CMIP3 models hindcasted decline trend, in which only BCC_CSM1.0.1 shows CI = 95% (Table 1). Neither CMIP5 nor CMIP3 Opt_T_Ens hindcasted the spatial pattern of the annual decline trend.

We sort out the optimal models in which the trends in seasonal mean NWS are relatively well correlated (PCC > 0.1 and trend < 0) to the observations in the sub-regions of NNW, NE, SW, CW and SSE of China (Table S3). The ensemble of seasonally optimal hindcasts by both CMIP3 and CMIP5 suggests that the decline trend occurs in all the seasons, but one order smaller than observations (Table S5). Winter has best hindcast compared to observations, followed by summer and spring. In consistent with observations, the ensemble of seasonally optimal CMIP5 hindcasts shows most significant decline trend in winter, but weakest in summer, which is not indicated by the ensemble of seasonally optimal CMIP3 hindcasts.

4. Discussions and conclusions

The spatial pattern of NWS is reproduced by most of CMIP5 and CMIP3 models. Most models in CMIP5 and CMIP3 underestimate annual mean NWS, but overestimate in southwestern China where the complex topography causes great uncertainties in hindcasts of NWS (Kumar *et al.*, 2015). The decline trends in both CMIP5

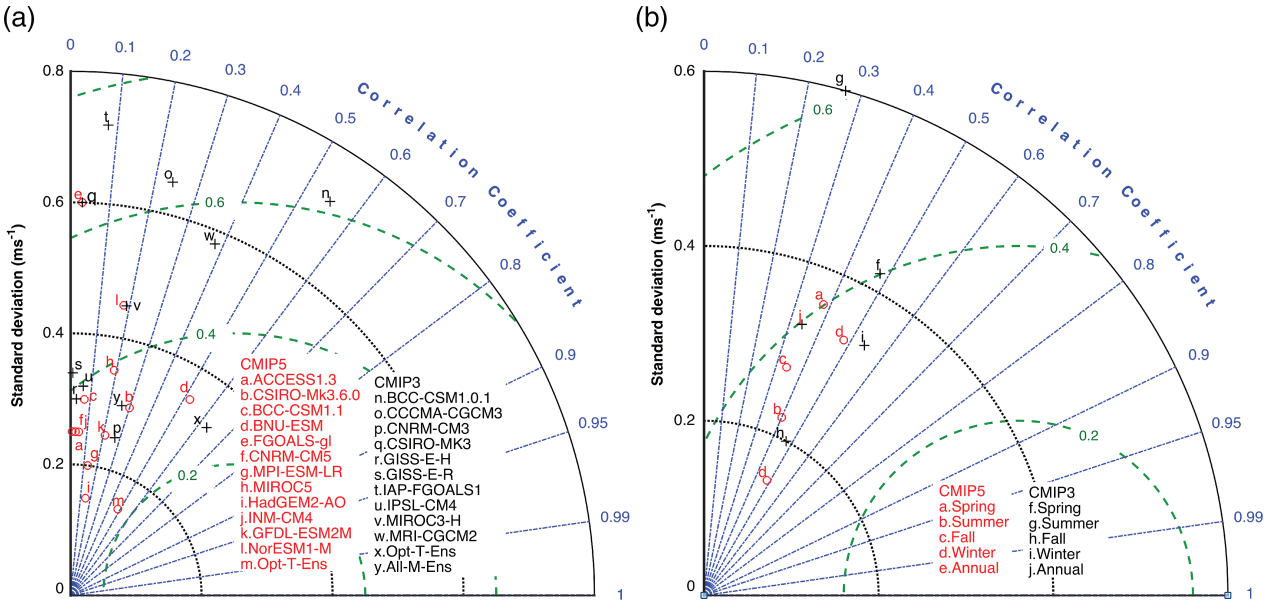

Figure 3. Taylor diagram comparing CMIP5 model hindcasts with observations for (a) annual mean wind speed in individual model and (b) seasonal mean wind speed in ensemble of optimal hindcast. The models and ensemble whose interannual variation of annual mean wind speed is positively correlated to observation are plotted in (a).

and CMIP3 are not well represented, which are smaller than observed decline trend by the magnitude of one order. Besides the temporal trend in mean NWS, CMIP models cannot represent the temporal trend of extreme wind (Kumar *et al.,* 2015).

CMIP5 shows improvements over CMIP3 in: (1) the number of optimal models that can hindcast spatial pattern and the decline trend of the mean NWS, (2) the magnitude and spatial pattern of the mean NWS and (3) the seasonal pattern of the decline trend. It is probably that the advantages of CMIP5 over CMIP3 are partly due to the shorter comparison period by CMIP3 models. Further, Kusunoki and Arakawa (2015) attributed the advantages of CMIP5 over CMIP3 in hindcasting east Asia precipitation to the higher horizontal resolution and improved representation of the west pacific subtropical high (WPSH) in CMIP5. We noticed that the models with higher resolution in CMIP5 show improvement in simulating spatial pattern and magnitude of NWS (Table S2). CMIP5 hindcasted smaller northward bias of WPSH than CMIP3 (Song and Zhou, 2014). The northward movement of WPSH directly affects the position and development of East Asia monsoon and Tropical cyclone activities (Chen *et al.,* 2004). The improved hindcasts of WPSH are highly associated with the improvement in the summer precipitation and monsoon circulation (Kusunoki and Arakawa, 2015) and significantly improved the wind at 850-hPa, which is also attributed to the better representation of the tropical eastern Indian Ocean-the western Pacific anticyclone teleconnection (Song and Zhou, 2014).

In the three reanalyses, ERA-interim is superior to ERA-40 and NCEP/NCAR in representing the spatial pattern of observed mean NWS. The correlation to observations of ERA-interim is just slightly smaller than CMIP5 optimal ensemble. However, similar to the most models, ERA-interim significantly underestimates the decline trend. Although NCEP/NCAR is the only dataset that has the mean NWS and decline trend close to observations, it is unable to represent the spatial pattern of mean NWS. The inability to represent the interannual variation and temporal trend of NWS was also reported in Australian NWS climatology (McVicar *et al.,* 2008).

It is encouraging that the ensembles, especially the ensemble of optimal model hindcasts outperforms individual model, although the models that can reproduce the spatial pattern of mean NWS are not skillful to represent the temporal trend of wind variation. The analyses presented here and in previous studies (McVicar *et al.,* 2008; Kumar *et al.,* 2015) reveal the uncertainties in wind field products including reanalyses and model outputs and highlight the benefits of parameterization development and increased horizontal resolution in the new-generation CMIP models. We expect to quantitatively evaluate the improvement in regional climate simulations by the integration of Global Monsoon MIP and High Resolution MIP experiments in CMIP6 (Eyring *et al.,* 2016).

The slowed winds trends are not well explained. The slowed East Asian monsoon winds may contribute to the decline trend in China, resulting from heterogeneous spatial and seasonal temperature variations and the net radiation and weakened incoming solar radiation (Xu *et al.,* 2006). The CMIP5 models fail to hindcast the decreasing trend of East Asia monsoon (Saha *et al.,* 2014). On the Tibetan Plateau, the warming may weaken the latitudinal gradients of regional temperature and surface pressure, thus altering the atmospheric circulation and reducing NWS (You *et al.,* 2014). However, the CMIP5 models cannot well represent the warming climate over Tibetan Plateau

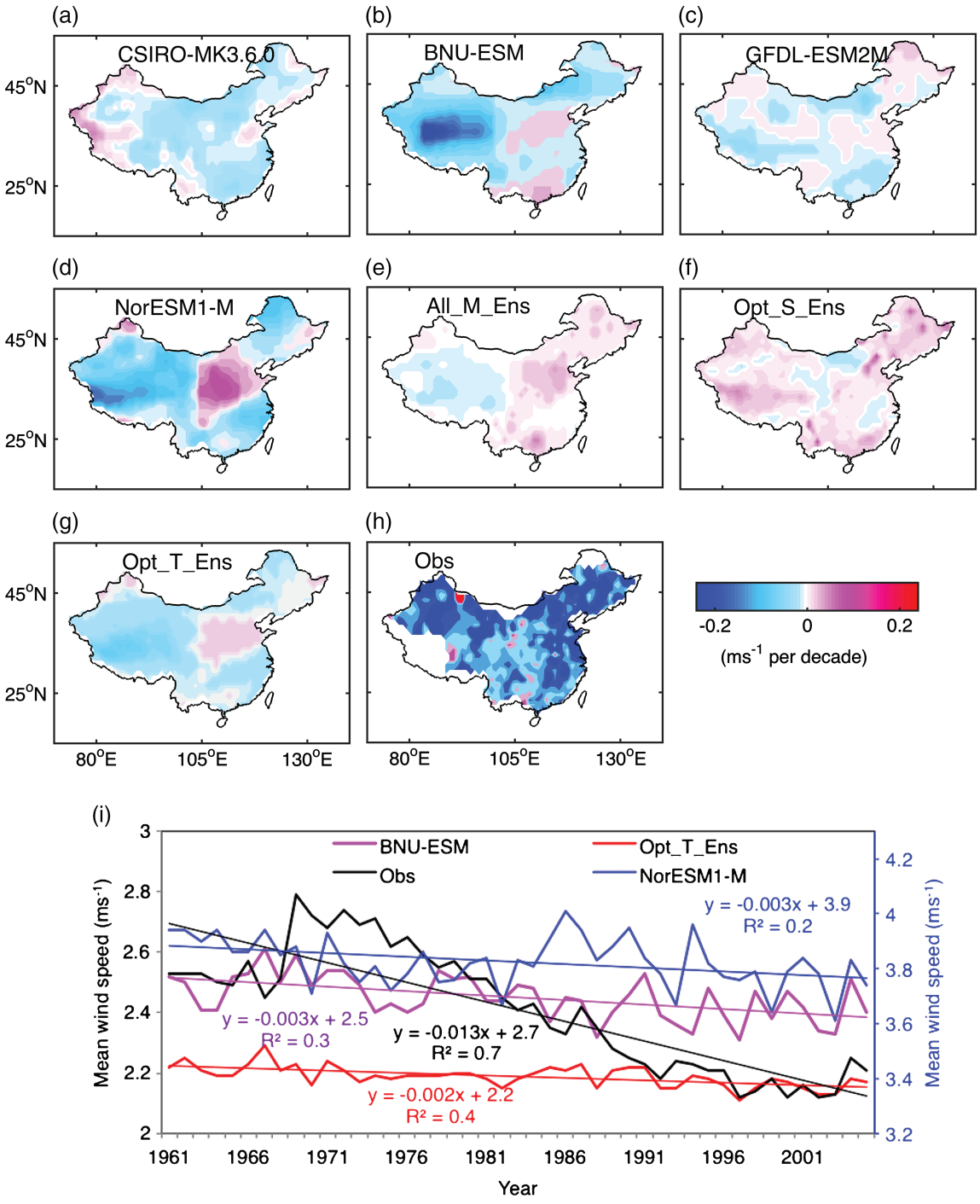

Figure 4. The hindcasts of wind trend in the optimal CMIP5 models that have good correlation to measured trend (a–d), ensembles (e–g), observations (h) over mainland China and time series of the annual mean wind speed in measurements, and the optimal models.

and underestimate the mean temperature significantly (Su *et al.*, 2013). In China, high afforestation rate of 1.5% leads to increases in surface roughness, which may explain 10–50% of the declined NWS (Vautard *et al.*, 2010). Urbanization also increases the surface roughness thus leads to declined NWS (Hou *et al.*, 2013). This time-evolving land-use change was not represented in CMIP3 but in CMIP5 (Taylor *et al.*, 2012). The historical land cover and land-use change in CMIP5 were provided through land-use harmonization based on Global Land Model (Di Vittorio *et al.*, 2014). This land cover dataset regrided from the History Database of the Global Environment (HYDE) database (Klein Goldewijk *et al.*, 2011) is unable to accurately represent the land-use change in China (Miao *et al.*, 2013). But, we are encouraged that the HYDE database is continuously updated with more reliable inventory data (Klein Goldewijk *et al.*, 2011). The Land Use Model Intercomparison Project (LUMIP) (Lawrence *et al.*, 2016) will enable quantitative evaluations of the climate responses to land use and land cover change.

Acknowledgements

This research is supported by the project (41205114) from the National Natural Science Foundation of China and grant from CAS Pioneer Hundred Talents Program. NCEP Reanalysis data provided by the NOAA/OAR/ESRL PSD, Boulder, Colorado, USA, from their Web site at http://www.esrl.noaa.gov/psd/. We acknowledge the World Climate Research Programme's Working Group on Coupled Modeling, which is responsible for CMIP, and we thank the climate modeling groups (listed in Table S2 of this paper) for producing and making available their model outputs. For CMIP, the U.S. Department of Energy's Program for Climate Model Diagnosis and Intercomparison provides coordinating support and led development of software infrastructure in partnership with the Global Organization for Earth System Science Portals.

We declare no conflict of interest.

Supporting information

The following supporting information is available:

Figure S1 The distribution of weather stations and subregions of China in this study: A. North-Northwestern (NNW), B. Northeastern (NE), C. Southwestern (SW), D. Central-Western (CW) and E. South-Eastern (SE).

Figure S2: Distributions of mean wind speed (averaged over 1961–2005) for individual model (a–w).

Figure S3. The model performance in hindcasting the annual and seasonal mean wind speed: (a) The percentage of models in which the wind speed biases are within $\pm 1.0\,ms^{-1}$, (b) The wind speed biases in ensembles by CMIP5 and CMIP3.

Figure S4. The seasonal and annual root mean square error (RMSE): CMIP3 *versus* CMIP5.

Table S1. The studies of the changes in near-surface wind speed in China (recreated from Zhao, 2016).

Table S2. The CMIP3 and CMIP5 models under evaluation.

Table S3. The models participating in the ensemble analysis.

Table S4. Model performance in hindcasts of seasonal and annual wind speed and correlations between seasonal ensembles and observations.

Table S5. The trend in simulated and hindcasted seasonal and annual mean wind in subregions (ms^{-1} per decade).

Appendix S1. Data information.

References

Berrisford P, Dee DP, Fielding K, Fuentes M, Kållberg P, Kobayashi S, Uppala SM. 2009. *The ERA-Interim Archive*. ERA Report Series, No. 1. ECMWF: Reading, UK.

Chen T-C, Wang S-Y, Huang W-R, Yen M-C. 2004. Variation of the east Asian summer monsoon rainfall. *Journal of Climate* **17**: 744–762.

Chen L, Pryor SC, Li D. 2012. Assessing the performance of Intergovernmental Panel on Climate Change AR5 climate models in simulating and projecting wind speeds over China. *Journal of Geophysical Research. Atmospheres* **117**: D24102. https://doi.org/10.1029/2012JD017533.

China Meteorological Administration (CMA). 2015. *China Climate Change Bulletin 2015*. Beijing: Science Press: Beijing. ISBN: 978-7-03-048283-9.

Di Vittorio AV, Chini LP, Bond-Lamberty B, Mao J, Shi X, Truesdale J, Craig A, Calvin K, Jones A, Collins WD, Edmonds J, Hurtt GC, Thornton P, Thomson A. 2014. From land use to land cover: restoring the afforestation signal in a coupled integrated assessment-earth system model and the implications for CMIP5 RCP simulations. *Biogeosciences* **11**: 6435–6450.

Eyring V, Bony S, Meehl GA, Senior CA, Stevens B, Stouffer RJ, Taylor KE. 2016. Overview of the coupled model Intercomparison project phase 6 (CMIP6) experimental design and organization. *Geoscientific Model Development* **9**: 1937–2958.

Font V. 2016. Wind energy setting records, growing still: the wind energy outlook for 2016. Renewable Energy World.

Hou A, Ni G, Yang H, Lei Z. 2013. Numerical analysis on the contribution of urbanization to wind stilling over the greater Beijing Metropolitan Area. *Journal of Applied Meteorology* **52**: 1105–1115.

Isaaks EH, Srivastava RM. 1989. *An Introduction to Applied Geostatistics*. Oxford University Press: New York, NY; 592.

Jiang Y, Luo Y, Zhao Z. 2010a. Projection of wind power density in China in the 21st century by climate models. *Chinese Geographical Science* **32**: 640–649.

Jiang Y, Luo Y, Zhao Z. 2010b. Evaluation of wind speeds in China as simulated by global climate models. *Acta Meteorologica Sinica* **67**: 1020–1029.

Kalnay E, Kanamitsu M, Kistler R, Collins W, Deaven D, Gandin L, Iredell M, Saha S, White G, Woollen J, Zhu Y, Leetmaa A, Reynolds R, Chelliah M, Ebisuzaki W, Higgins W, Janowiak J, Mo KC, Ropelewski C, Wang J, Jenne R, Joseph D. 1996. The NCEP/NCAR 40-year reanalysis project. *Bulletin of the American Meteorological Society* **77**: 437–470.

Klein Goldewijk K, Beruen A, Gerard Drecht V, Martine Vos D. 2011. The HYDE 3.1 spatially explicit database of human-induced global land-use change over the past 12,000 years. *Global Ecology and Biogeography* **20**: 73–86.

Kumar D, Mishra V, Ganguly AR. 2015. Evaluating wind extremes in CMIP5 climate models. *Climate Dynamics* **45**: 441–453.

Kusunoki S, Arakawa O. 2015. Are CMIP5 models better than CMIP3 models in simulating precipitation over East Asia. *Journal of Climate* **28**: 5601–5621.

Lawrence DM, Hurtt GC, Arneth A, Brovkin V, Calvin KV, Jones AD, Jones CD, Lawrence PJ, de Noblet-Ducoudré N, Pongratz J, Seneviratne SI, Shevliakova E. 2016. The land use model intercomparison project (LUMIP) contribution to CMIP6: rationale and experimental design. *Geoscientific Model Development* **9**: 2973–2998.

Lynch AH, Curry JA, Brunner RD, Maslanik JA. 2004. Toward an integrated assessment of the impacts of extreme wind events on Barrow, Alask. *Bulletin of the American Meteorological Society* **85**: 209–221.

McVicar TR, van Niel TG, Li L, Roderick ML, Rayner DP, Ricciardulli L, Donohue RJ. 2008. Wind speed climatology and trends for Australia, 1957-2006: capturing the stilling phenomenon and comparison with near-surface reanalysis output. *Geophysical Research Letters* **35**: L20403. https://doi.org/10.1029/2008GL035627.

Meehl GA, Covey C, Delworth T, Latif M, McAvaney B, Mitchell JFB, Stouffer RJ, Taylor KE. 2007. The WCRP CMIP3 multi-model dataset: a new era in climate change research. *Bulletin of the American Meteorological Society* **88**: 1383–1394.

Miao L, Zhu F, He B, Ferrat M, Liu Q, Cao X, Cui X. 2013. Synthesis of China's land use in the past 300 years. *Global and Planetary Change* **100**: 224–233.

Ogata T, Ueda H, Inoue T, Hayasaki M, Yoshida A, Watanabe S, Kira M, Ooshiro M, Kumai A. 2014. Projected future changes in the Asian monsoon: a comparison of CMIP3 and CMIP5 model results. *Journal of the Meteorological Society of Japan. Ser. II* **92**: 207–225.

Pryor SC, Barthelmie RJ, Young DT, Takle ES, Arritt RW, Flory D, Gutowski WJ Jr, Nunes A, Roads J. 2009. Wind speed trends over the contiguous United States. *Journal of Geophysical Research. Atmospheres* **114**: D14105. https://doi.org/10.1029/2008JD011416.

Pryor SC, Barthelmie RJ, Clausen NE, Drews M, MacKellar N, Kjellström E. 2012. Analyses of possible changes in intense and extreme wind speeds over northern Europe under climate change scenarios. *Climate Dynamics* **38**: 189–208.

Ren D. 2010. Effects of global warming on wind energy availability. *Journal of Renewable and Sustainable Energy* **2**: 052301. https://doi.org/10.1063/1.3486072.

Saha A, Ghosh S, Sahana AS, Rao EP. 2014. Failure of CMIP5 climate models in simulating post-1950 decreasing trend of Indian monsoon. *Geophysical Research Letters*, **41**: 7323–7330. https://doi.org/10.1002/2014GL061573.

Song F, Zhou T. 2014. Interannual variability of east Asian summer monsoon simulated by CMIP3 and CMIP5 AGCMs: skill dependence on Indian ocean-western Pacific anticyclone teleconnection. *Journal of Climate* **27**: 1679–1697.

Su F, Duan X, Chen D, Hao Z, Cuo L. 2013. Evaluation of the global climate models in the CMIP5 over the Tibetan Plateau. *Journal of Climate* **26**, 3187–3208.

Sperber KR, Annamalai H, Kang I-S, Kitoh A, Moise A, Turner A, Wang B, Zhou T. 2013. The Asian summer monsoon: an intercomparison of CMIP5 vs. CMIP3 simulations of the late 20th century. *Climate Dynamics* **41**: 2711–2744.

Taylor KE, Stouffer RJ, Meehl GA. 2012. An overview of CMIP5 and the experimental design. *Bulletin of the American Meteorological Society* **93**: 485–498.

Uppala SM, KÅllberg PW, Simmons AJ, Andrae U, Bechtold VDC, Fiorino M, Gibson JK, Haseler J, Hernandez A, Kelly GA, Li X, Onogi K, Saarinen S, Sokka N, Allan RP, Andersson E, Arpe K, Balmaseda MA, Beljaars ACM, Berg LVD, Bidlot J, Bormann N, Caires S, Chevallier F, Dethof A, Dragosavac M, Fisher M, Fuentes M, Hagemann S, Hólm E, Hoskins BJ, Isaksen L, Janssen PAEM, Jenne R, Mcnally AP, Mahfouf J-F, Morcrette J-J, Rayner NA, Saunders RW, Simon P, Sterl A, Trenberth KE, Untch A, Vasiljevic D, Viterbo P, Woollen J. 2005. The ERA-40 re-analysis. *Quarterly Journal of the Royal Meteorological Society* **131**: 2961–3012.

Vautard R, Cattiaux J, Yiou P. 2010. Northern hemisphere atmospheric stilling partly attributed to an increase in surface roughness. *Nature Geoscience* **3**: 756–761.

Xu M, Chang C-P, Fu C, Qi Y, Robock A, Robinson D, Zhang H. 2006. Steady decline of east Asian monsoon winds, 1969-2000: evidence from direct ground measurements of wind speed. *Journal of Geophysical Research. Atmospheres* **111**: D24111. https://doi.org/10.1029/2006JD007337.

You Q, Kang S, Flügel W-A, Pepin N, Yan Y, Huang J. 2010. Decreasing wind speed and weakening latitudinal surface pressure gradients in the Tibetan plateau. *Climate Research* **42**: 57–63. https://doi.org/10.3354/cr00864.

You Q, Fraedrich K, Min J, Kang S, Zhu X, Pepin N, Zhang L. 2014. Observed surface wind speed in the Tibetan plateau since 1980 and its physical causes. *International Journal of Climatology* **34**: 1873–1882.

Zhao Z, Luo Y, Jiang Y, Huang J. 2016. Possible reasons of wind speed decline in China for the last 50 years. *Advances in Meteorological Science and Technology* **6**, 106–109.